Supplement of Hydrol. Earth Syst. Sci., 25, 1009–1032, 2021
https://doi.org/10.5194/hess-25-1009-2021-supplement

Hydrology and
Earth System
Sciences
Open Access

Supplement of

Lake thermal structure drives interannual variability in summer anoxia dynamics in a eutrophic lake over 37 years

Robert Ladwig et al.

Correspondence to: Robert Ladwig (rladwig2@wisc.edu)

Supplementary material

PIHM-Lake description

PIHM-Lake is built upon a physically-based spatially distributed hydrologic model—PIHM (Penn State Integrated Hydrologic Model) (Qu and Duffy, 2007)—with the capability of simulating surface, subsurface, and channel water exchange between a catchment and a lake, as well as the water level change of the lake. As illustrated in Supplement Figure S11, PIHM-Lake model uses a finite volume numerical scheme and unstructured triangular mesh to represent the domain. It tracks the changes of surface and subsurface water storage on a 3D catchment and 1D lake as a function of precipitation, evapotranspiration, recharge, surface and groundwater flow, channelized flow, and snow melt. The spatial variation of overland flow and groundwater flow between the catchment and the lake is characterized by the water flows through the edges of each triangular mesh. Specifically, based on the conservation of mass of water, the generic form of the governing equations for PIHM-Lake is

$$\begin{cases} \frac{dS_{canopy}}{dt} = vFrac * (1 - sFrac) * P - E_c \\ \frac{dS_{snow}}{dt} = sFrac * P - SM \\ \frac{\partial S_{surf}}{\partial t} = TF - \nabla q_{sw} - I - E_s \\ \frac{dS_{unsat}}{dt} = I - R - E_g - E_{gt} \\ \frac{\partial S_{sat}}{\partial t} = -\nabla q_{gw} + R - E_{sat} - E_{tsat} \end{cases} \tag{1}$$

where $\frac{dS_{canopy}}{dt}$ = the time rate of change of the canopy water storage, S_{canopy} (m), due to canopy evaporation E_c (m/day) and canopy interception $vFrac * (1 - sFrac) * P$ (m/day). $vFrac$ and $sFrac$ are the vegetation fraction and snow fraction, respectively. P = precipitation (m/day). $\frac{dS_{snow}}{dt}$ = the time rate of change of snow storage S_{snow} (m) due to $sFrac * P$:snow formation from precipitation when temperature is below 0 °C (m/day) and SM, snow melt (m/day), which is a function of degree-day factor of ice and snow melt. $\frac{\partial S_{surf}}{\partial t}$ =the time rate of change of surface water storage, S_{surf} (m), due to TF=

throughfall (m/day), ∇q_{sw}= net overland flow (m/day), I: infiltration (m/day), and E_s: surface water evaporation (m/day). ∇q_{sw} is modeled by the diffusion wave approximation of St. Venant's equation assuming shallow surface water depth and negligible influence of inertia force on overland flow, which is equivalent to Manning's equation. The estimation of infiltration rate is a function of the gradient of the surface and subsurface hydraulic head. $\frac{dS_{unsat}}{dt}$ represents the time rate of change of unsaturated water storage (m) due to I: infiltration (m/day), R: recharge (m/day), E_g: soil evaporation (m/day), and E_{gt}: transpiration (m/day). The recharge is calculated using Richard's equation assuming a vertical exchange of water across a moving water table interface. $\frac{\partial S_{sat}}{\partial t}$ = the time rate of change of S_{sat}: the saturated water storage (m). ∇q_{gw} = net groundwater lateral movement between adjacent cells (m/day) is represented by the Darcy-type flow proportional to groundwater gradient. E_c, E_s, E_g and E_{sat} are the evaporation (m/day) from the vegetation canopy, surface water, unsaturated and saturated soil zone, respectively. The potential evaporation rate is estimated by the Penman equation. The transpiration (m/day) is described by E_{gt} or E_{tsat}, depending upon the vegetation coverage, the rooting depth and the groundwater table. If the groundwater table is higher than rooting depth, plants uptake water from the saturated zone, and E_{tsat} applies. Otherwise, water uptake occurs at the unsaturated soil zone, and E_{gt} applies.

For the hydrodynamics of the 1-D lake, we consider a two-layer system: a surface water layer and an aquifer layer. Surface water flow between the catchment boundary cells directly affects the water storage of surface water layer. Meanwhile, subsurface water flows through the aquifer layer and indirectly contributes to surface water through negative recharge. Likewise, based on the conservation of mass of water, the governing equation for the 1D lake component is

$$\begin{cases} \frac{\partial S_{lake\_surf}}{\partial t} = P - E_s - R + q_{sw} \\ \frac{\partial S_{lake\_gw}}{\partial t} = R + q_{gw} \end{cases} \tag{2}$$

where $\frac{\partial S_{lake\_surf}}{\partial t}$ = the time rate of change of lake surface water. $\frac{\partial S_{lake\_gw}}{\partial t}$ = the time rate of change of water storage in lake bottom aquifer. P =precipitation (m/day); E_s = surface water evaporation (m/day); R = recharge (m/day). A positive value of R indicates downward lake surface water, while a negative value indicates an upward groundwater recharge to surface water; q_{sw} and q_{gw} are surface and groundwater flow through the edges of the lake boundary, respectively.

Details of the model processes and code is referred to the model repository: https://github.com/hydro-geomorph-zhang/PIHM-Lake.

Figures

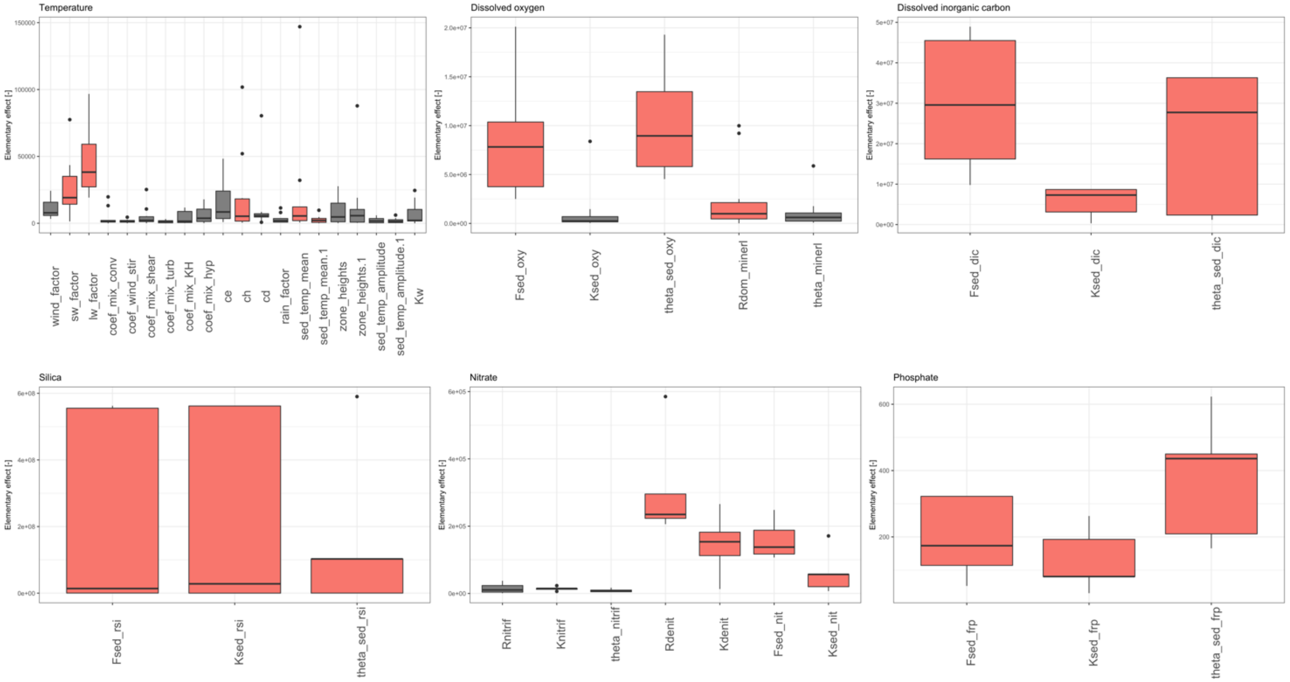

Figure S1 Mean and standard deviations of absolute elementary effects quantified by the Morris Method for water temperature, dissolved oxygen, dissolved inorganic carbon, silica, nitrate and phosphate. Colored bars are sensitive parameters that were used in the calibration.

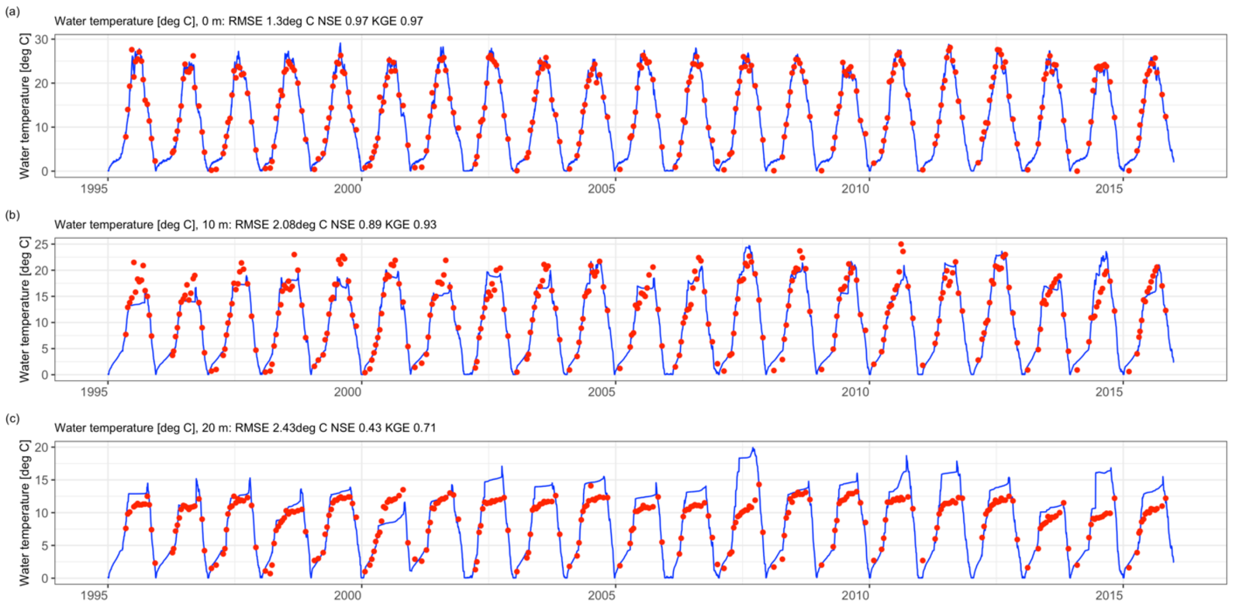

Figure S2 Time-series comparison between observed (red dots) and water temperatures (blue lines). The fit criteria root-mean square error (RMSE), Nash-Sutcliffe coefficient of efficiency (NSE) and Kling-Gupta coefficient of efficien

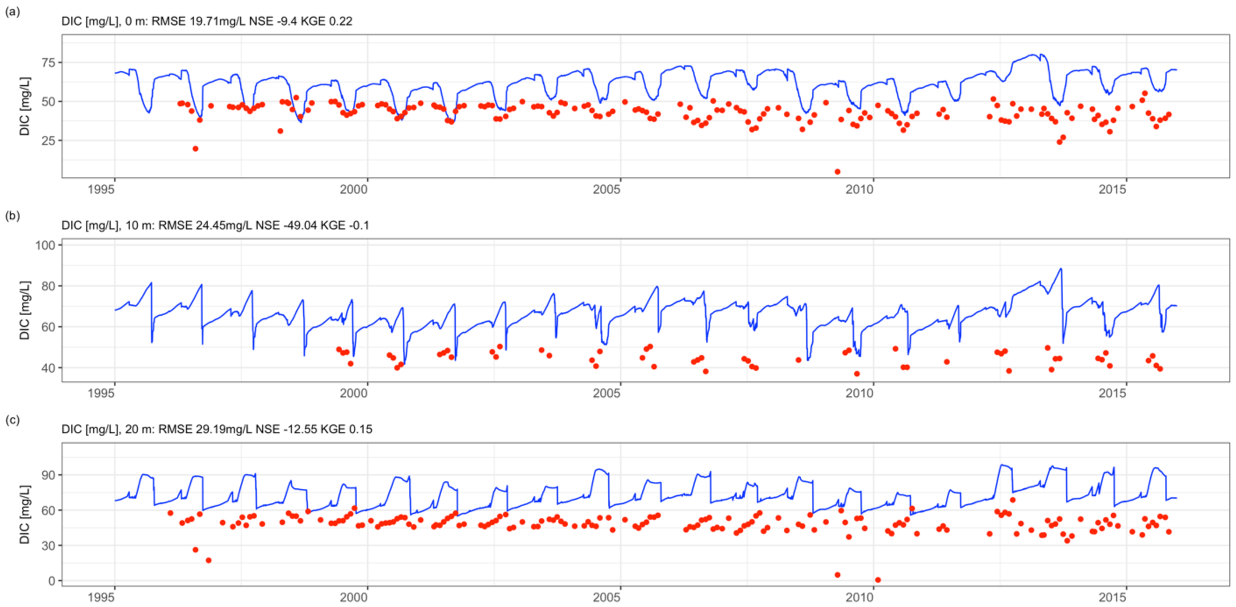

Figure S3 Time-series comparison between observed (red dots) and modeled dissolved inorganic carbon concentrations (blue lines). The fit criteria root-mean square error (RMSE), Nash-Sutcliffe coefficient of efficiency (NSE) and Kling-Gupta coefficient of efficiency (KGE).

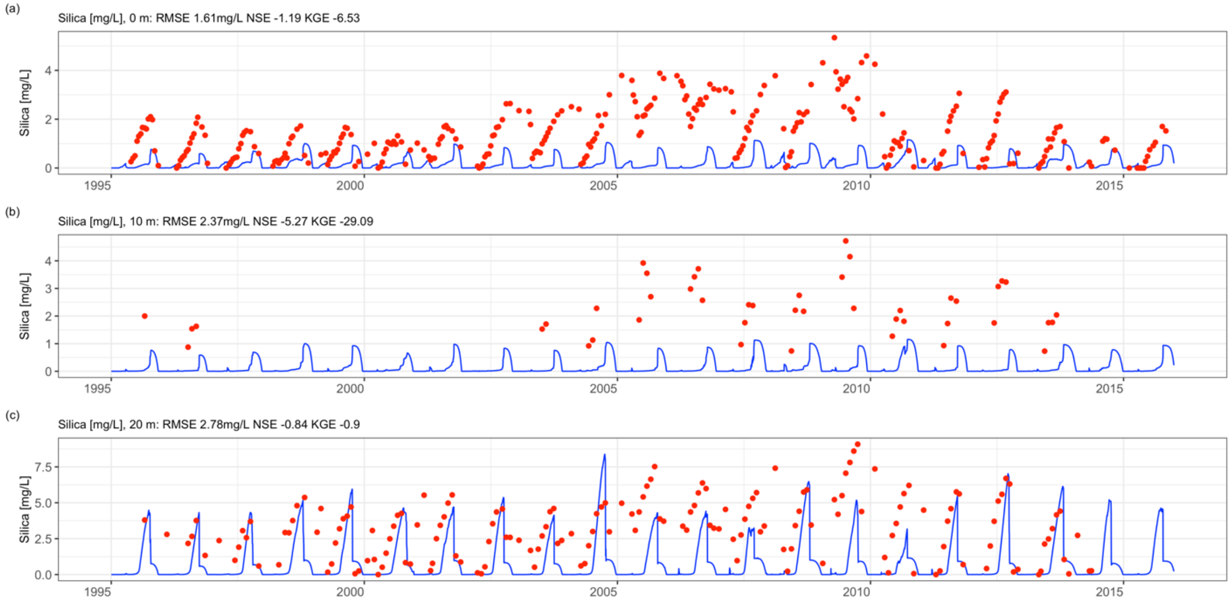

Figure S4 Time-series comparison between observed (red dots) and modeled silica concentrations (blue lines). The fit criteria root-mean square error (RMSE), Nash-Sutcliffe coefficient of efficiency (NSE) and Kling-Gupta coefficient of efficiency (KGE).

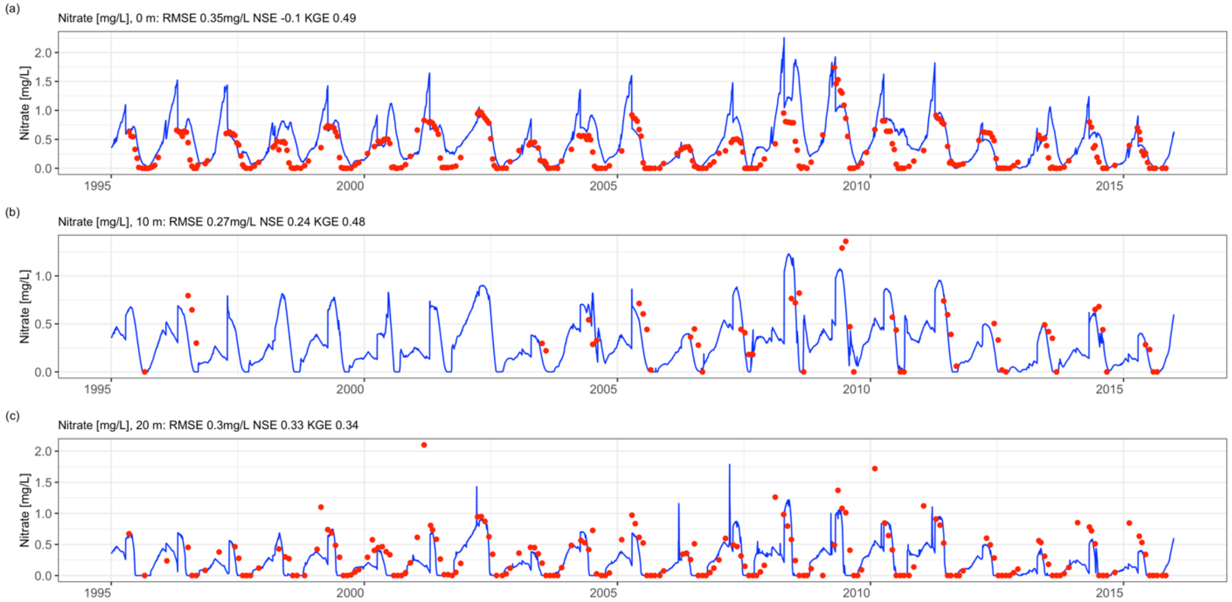

Figure S5 Time-series comparison between observed (red dots) and modeled nitrate concentrations (blue lines). The fit criteria root-mean square error (RMSE), Nash-Sutcliffe coefficient of efficiency (NSE) and Kling-Gupta coefficient of efficiency (KGE).

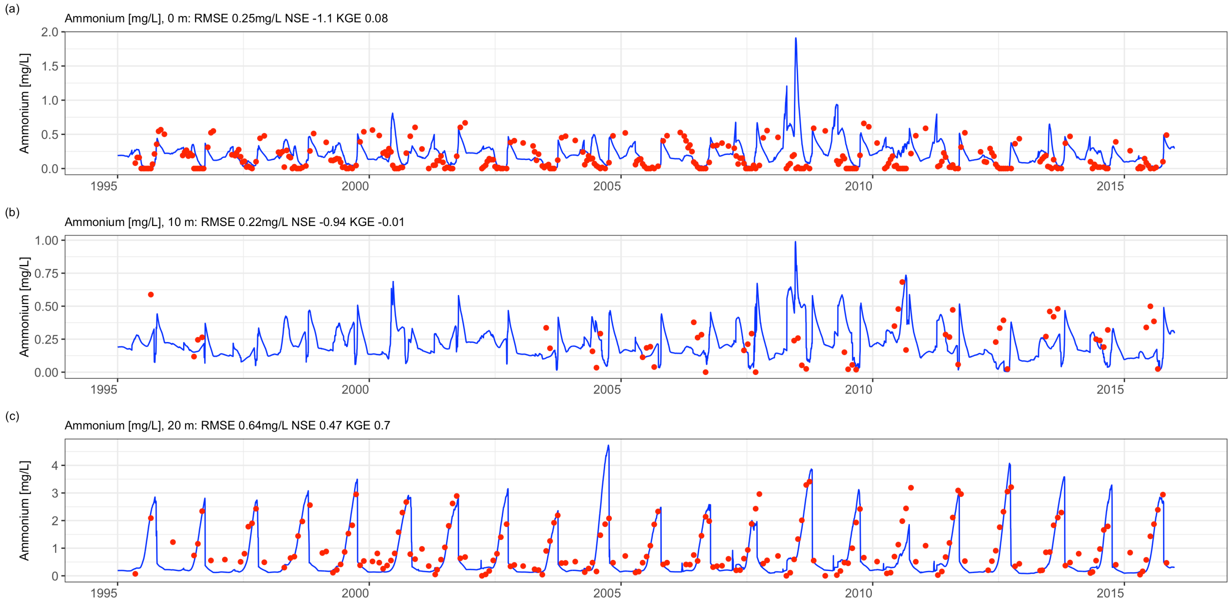
(a) Ammonium [mg/L], 0 m: RMSE 0.25mg/L NSE -1.1 KGE 0.08

(b) Ammonium [mg/L], 10 m: RMSE 0.22mg/L NSE -0.94 KGE -0.01

(c) Ammonium [mg/L], 20 m: RMSE 0.64mg/L NSE 0.47 KGE 0.7

Figure S6 Time-series comparison between observed (red dots) and modeled ammonium concentrations (blue lines). The fit criteria root-mean square error (RMSE), Nash-Sutcliffe coefficient of efficiency (NSE) and Kling-Gupta coefficient of efficiency (KGE).

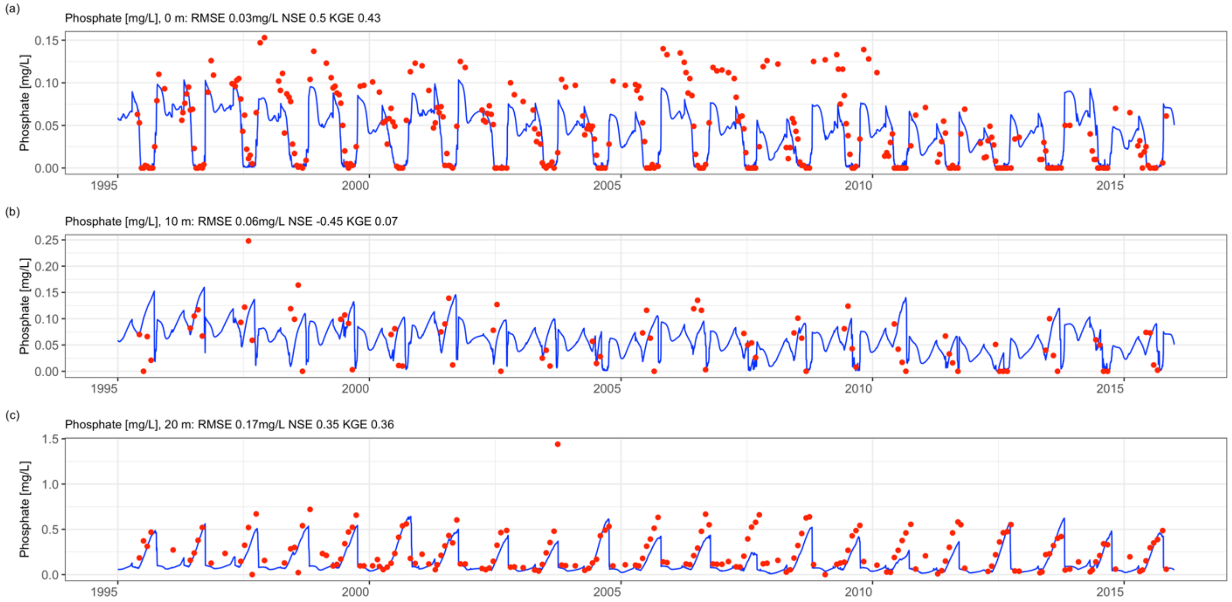
(a) Phosphate [mg/L], 0 m: RMSE 0.03mg/L NSE 0.5 KGE 0.43

(b) Phosphate [mg/L], 10 m: RMSE 0.06mg/L NSE -0.45 KGE 0.07

(c) Phosphate [mg/L], 20 m: RMSE 0.17mg/L NSE 0.35 KGE 0.36

Figure S7 Time-series comparison between observed (red dots) and modeled phosphate concentrations (blue lines). The fit criteria root-mean square error (RMSE), Nash-Sutcliffe coefficient of efficiency (NSE) and Kling-Gupta coefficient of efficiency (KGE).

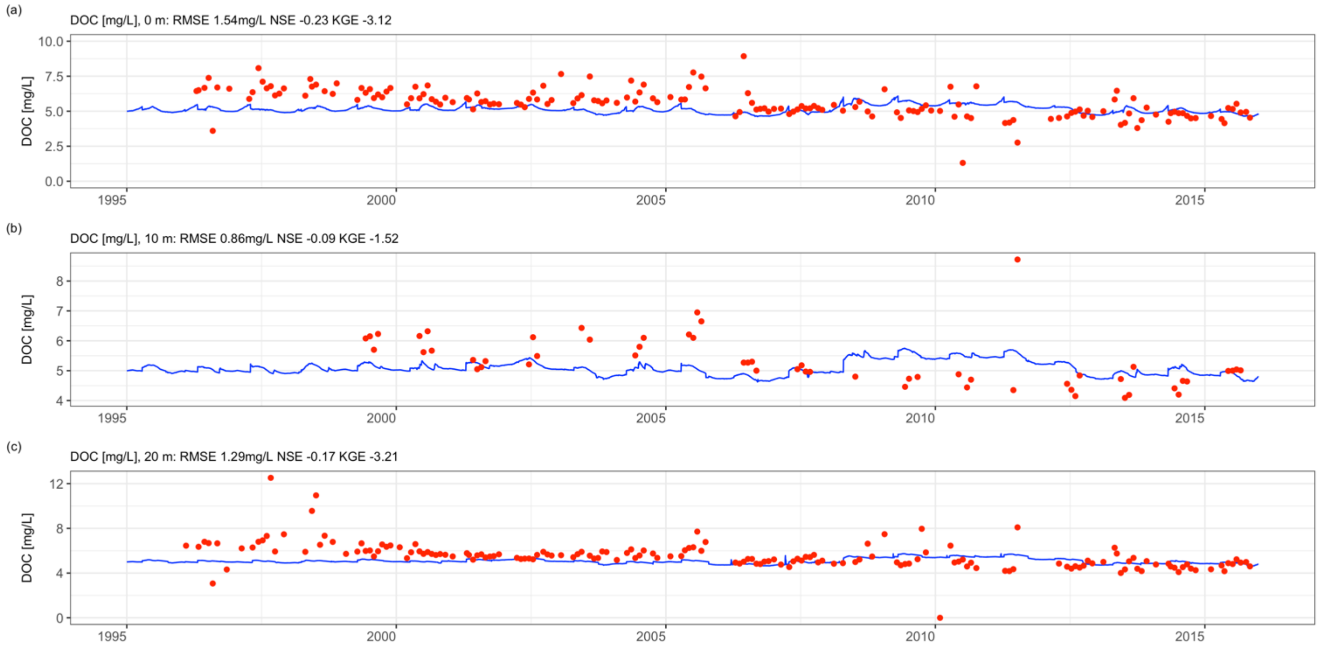

Figure S8 Time-series comparison between observed (red dots) and modeled dissolved organic carbon concentrations (blue lines). The fit criteria root-mean square error (RMSE), Nash-Sutcliffe coefficient of efficiency (NSE) and Kling-Gupta coefficient of efficiency (KGE).

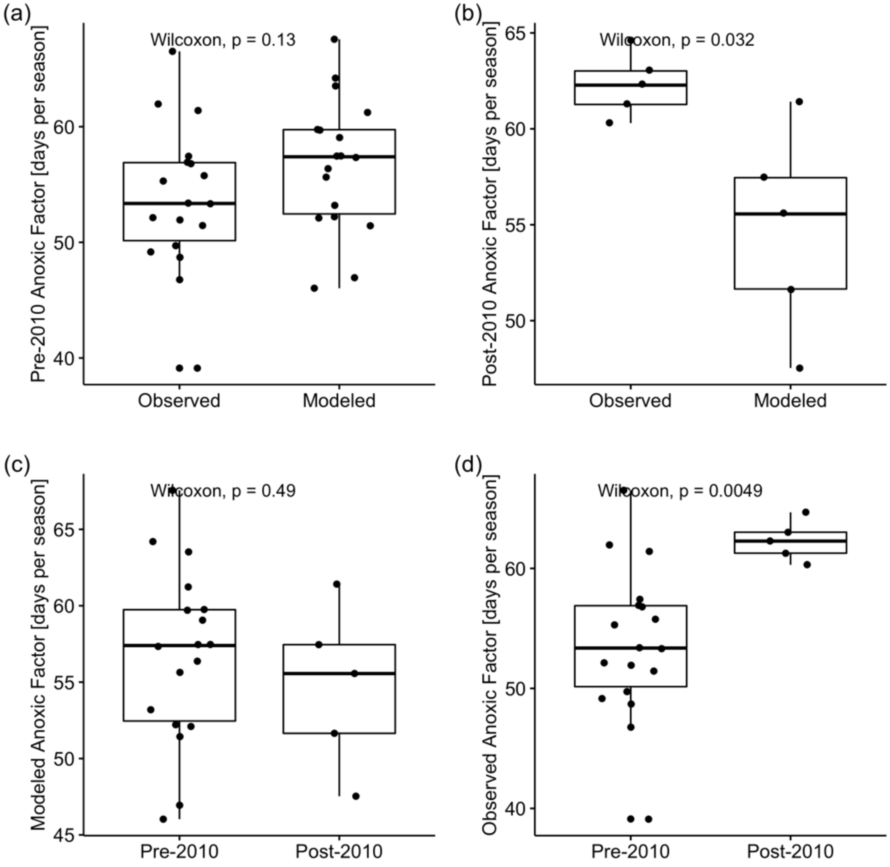

Figure S9 Box-whisker plots of (a) observed to modeled Anoxic Factors for the pre-2010 period 1992-2009, (b) observed to modeled Anoxic Factors for the post-2010 period 2010-2015, (c) pre- to post-2010 modeled Anoxic Factors, and (d) pre- to post-2010 observed Anoxic Factors.

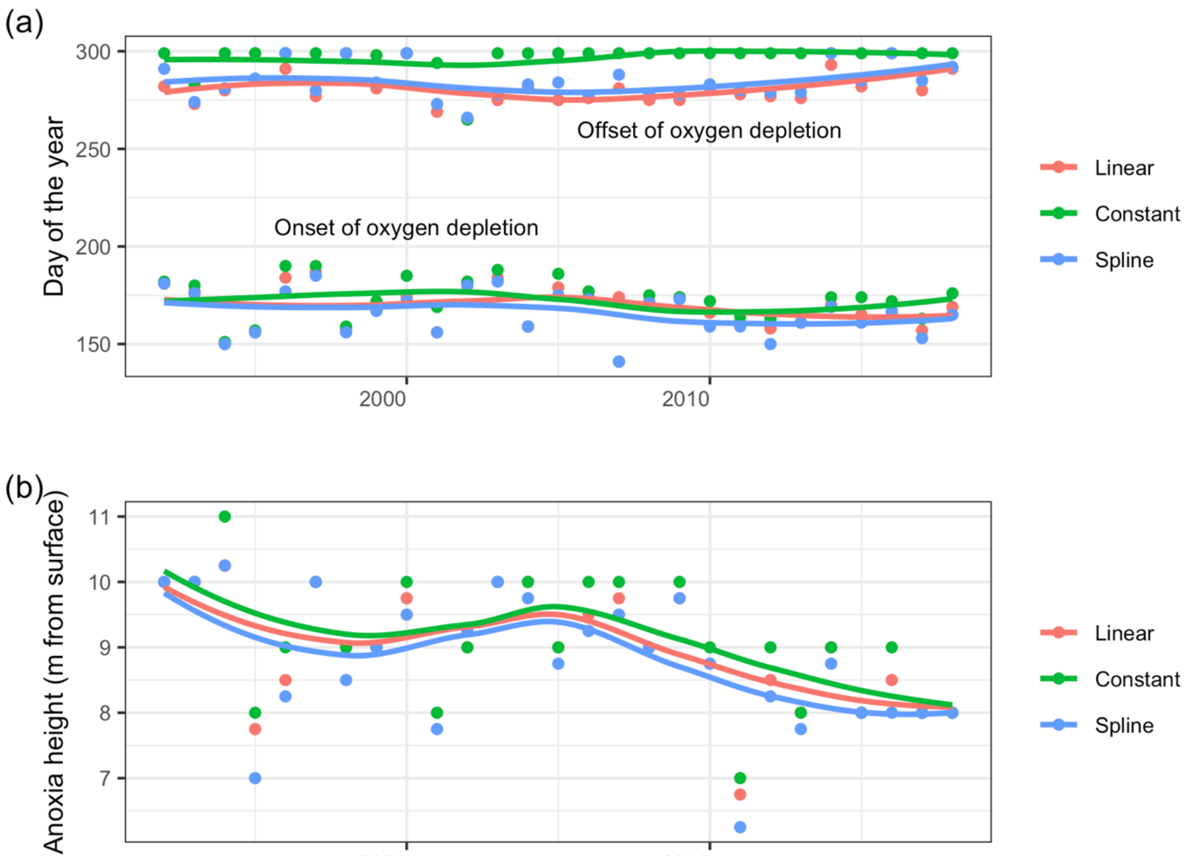

Figure S10 Observed anoxia onset, offset (a) and height (b) dynamics. The colored lines refer to the interpolation method.

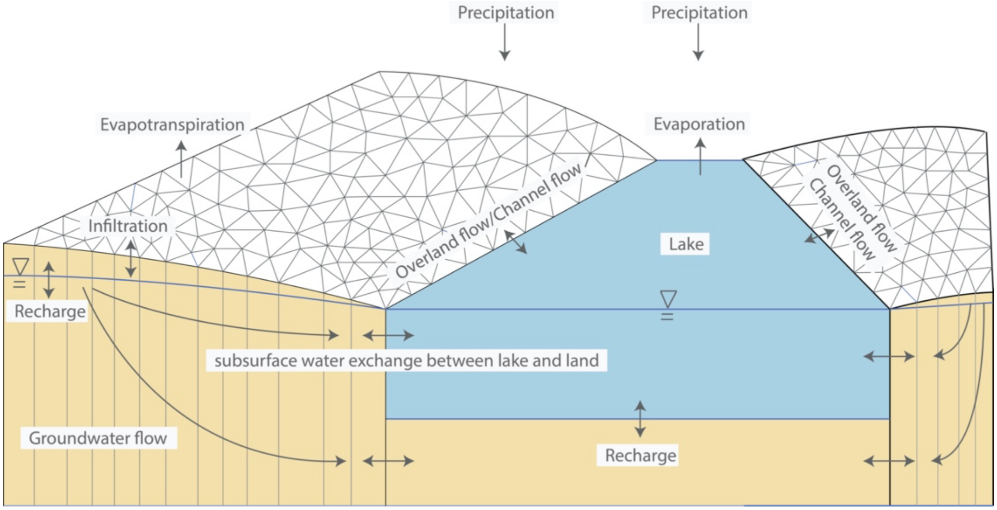

80 Figure S11 Conceptual framework of PIHM-Lake.

Tables

Table S1 Model parameters for functional phytoplankton groups

Parameter	Description	Cyanobacteria	Diatoms
P_initial	Initial concentration of phytoplankton (mmol C/m3)	10	8.4
P0	Minimum concentration of phytoplankton (mmol C/m3)	0.03	0.03
W_p	sedimentation rate (m/d)	0	-0.05
Xcc	carbon to chlorophyll ratio (mg C/mg chla)	50	50
R_growth	Phyto max growth rate @20C (/day)	0.8	2.8
fT_Method	Temperature limitation function of growth	CAEDYM style	CAEDYM style
Theta_growth	Arrhenius temperature scaling for growth function (-)	1.06	1.06
T_std	Standard temperature (deg C)	20	15
T_opt	Optimum temperature (deg C)	28	20
T_max	Maximum temperature (deg C	35	32
lightModel	Type of light response function	no photoinhibition	no photoinhibition
I_K	Half saturation constant for light limitation of growth (microE/m^2/s)	25	10

KePHY	Specific attenuation coefficient ((mmol C m^3^-1)^1 m^-1)	0.005	0.001
F_pr	Fraction of primary production lost to exudation (-)	0.005	0.002
R_resp	Phytoplankton respiration/metabolic loss rate @ 20 (deg C)	0.08	0.12
Theta_resp	Arrhenius temperature scaling factor for respiration (-)	1.05	1.07
K_fres	Fraction of metabolic loss that is true respiration (-)	0.6	0.6
K_fdom	Fraction of metabolic loss that is DOM (-)	0.05	0.05
simDINUptake	Simulate DIN uptake	True	True
simINDynamics	Simulate internal N	Fixed C:N	Dynamic C:N
N_0	Nitrogen concentration below which uptake is 0 (mmol N/m^3)	0	0
K_N	Half-saturation concentration of nitrogen (mmol N/m^3)	1	3.5
X_ncon	Constant internal nitrogen concentration (mmol N/ mmol C)	0.035	0.035
X_nmin	minimum internal nitrogen concentration (mmol N/ mmol C)	0.06	0.077
X_nmax	maximum internal nitrogen concentration (mmol N/ mmol C)	0.206	0.129
R_nuptake	maximum nitrogen uptake rate (mmol N/m^3/d)	0.068	0.13
R_nfix	nitrogen fixation rate (mmol N/mmol C/day)	0.13	0
simDIPUptake	Simulate DIP uptake	True	True
simIPDynamics	Simulate internal phosphorus dynamics	Dynamic C:P	Dynamic C:P
P_0	Phosphorus concentration below which uptake is 0 (mmol P/m^3)	0	0
K_P	Half-saturation concentration of phosphorus (mmol P/m^3)	0.5	0.7
X_pmin	Minimum internal phosphorus concentration (mmol P/mmol C)	0.0019	0.0081

X_pmax	Maximum internal phosphorus concentration (mmol P/mmol C)	0.0089	0.033
R_puptake	Maximum phosphorus uptake rate (mmol P/m^3/d)	0.0039	0.007
simSIUptake	Simulate Si uptake	False	True
Si_0	Silica concentration below which uptake is 0 (mmol Si/m^3	-	0
K_Si	Half-saturation concentration of silica (mmol Si /m3)	-	2.5
X_sicon	Constant internal silica concentration (mmol Si/mmol C)	-	0.04

Table S2 Calibrated model parameters

Parameter	Description	Unit	Default value (Hipsey et al., 2019a, 2019b)	Model value
f_{sw}	Solar radiation scaling factor	-	1.0	0.84
f_{lw}	Long-wave radiation scaling factor	-	1.0	0.99
C_H	Bulk aerodynamic coefficient for sensible heat transfer	-	0.0013	0.0014
$T_{z=1,mean}$	Annual mean temperature of the upper sediment zone	°C	-	5.07
$T_{z=2,mean}$	Annual mean temperature of the lower sediment zone	°C	-	13.47
F_{max}^{oxy}	Max. sediment flux for dissolved oxygen	$\frac{mmol}{m^2d^2}$	-100.0	-100.0
K_{sed}^{oxy}	Half-saturation concentration controlling oxygen sediment flux	$\frac{mmol}{m^3}$	50.0	15.0
θ_{sed}^{oxy}	Temperature multiplier for oxygen sediment flux	-	1.0	1.08

$R_{mineral}^{dom}$	Maximum rate of aerobic mineralisation of labile dissolved organic matter at 20 °C	d^{-1}	0.5	0.5
F_{max}^{dic}	Max. sediment flux for dissolved inorganic carbon (DIC)	$\frac{mmol}{m^2d^2}$	4.0	250.0
K_{sed}^{dic}	Half-saturation concentration controlling DIC sediment flux	$\frac{mmol}{m^3}$	30.0	7.0
θ_{sed}^{dic}	Arrhenius temperature multiplier for DIC sediment flux	-	1.0	1.08
F_{max}^{rsi}	Max. sediment flux for reactive silica	$\frac{mmol}{m^2d^2}$	-	16.42
K_{sed}^{rsi}	Half-saturation concentration controlling silica sediment flux	$\frac{mmol}{m^3}$	50.0	1.90
θ_{sed}^{rsi}	Arrhenius temperature multiplier for silica sediment flux	-	1.0	1.08
R_{nitrif}	Maximum rate of nitrification at 20 °C	d^{-1}	0.1	0.03
R_{denit}	Maximum rate of denitrification at 20 °C	d^{-1}	0.3	2.0
K_{denit}	Half-saturation concentration for denitrification	$\frac{mmol}{m^3}$	2.0	3.0
F_{max}^{nit}	Max. sediment flux for nitrate		-5.0	-9.55
K_{sed}^{nit}	Half-saturation concentration controlling nitrate sediment flux	$\frac{mmol}{m^3}$	100.0	173.13
F_{max}^{frp}	Max. sediment flux for phosphate	$\frac{mmol}{m^2d^2}$	-	0.49

K_{sed}^{frp}	Half-saturation concentration controlling phosphate sediment flux	$\frac{mmol}{m^3}$	-	200.0
θ_{sed}^{frp}	Arrhenius temperature multiplier for phosphate sediment flux	-	1.0	1.0

Table S3 Step-wise model-selection by removing predictors of the multiple linear regression model using seven predictors.

Predictor	AIC
HBR ratio during spring *(Spring.HBR)*	-61.820
HBR ratio during summer *(Summer.HBR)*	-60.529
Birgean Work during spring *(Spring.Birgean)*	-60.189
Gross primary production in the epilimnion (*Epi.GPP*)	-58.952
Schmidt Stability during summer *(Summer.St)*	-51.829
Birgean Work during summer *(Summer.B)*	-50.848
Onset of stratification *(Onset.Strat)*	-42.900

Table S4 Most parsimonious multiple linear regression model (adjusted $R^2 = 0.84$, $p < 0.001$) explaining the summer Anoxic Factor.

	Estimate	Std. Error	t value	Pr(>|t|)	Rel. importance [%]
Intercept	-1.04e-15	5.70e-2	0.00	1.00	
Schmidt Stability during summer *(Summer.St)*	5.386e-1	7.920e-2	6.800	3.23e-7	43
Onset of stratification *(Onset.Strat)*	-4.581-1	9.006e-2	-5.086	2.68e-5	42
Gross primary production in the epilimnion (*Epi.GPP*)	2.436e-1	8.327e-2	2.926	0.00704	15